Supporting Information

Slow magnetic relaxation in mononuclear octa-coordinate Fe(II) and Co(II) complexes from Bpybox ligand

Rui-Xia Li,[a] Hui-Ying Sun,[a] Hai-Chao Liang,[b] Cheng Yi,[a] Nian-Tao Yao,[a] Yin-Shan Meng,[a] Jin Xiong,*[c] Tao Liu,*[,a] and Yuan-Yuan Zhu*[,a,b]

*E-mail: yyzhu@hfut.edu.cn; jinxiong@andrew.cmu.edu; liutao@dlut.edu.cn

[a]*State Key Laboratory of Fine Chemicals, Dalian University of Technology, 2 Linggong Road, Dalian 116024, China.*

[b]*School of Chemistry and Chemical Engineering, Hefei University of Technology and Anhui Key Laboratory of Advanced Functional Materials and Devices, Hefei 230009, China.*

[c]*Department of Chemistry, Carnegie Mellon University, Pittsburgh, PA 15213, USA.*

Contents

SI1 Instruments and materials

SI1.1 Instruments

Structural characterization measurements. The NMR spectra were recorded on a Bruker 600 MHz spectrometer. Elemental analysis of carbon, nitrogen and hydrogen was performed using an Elementary Vario EL analyser. Mass spectrometry was performing using a Water XEVO G2Q-TOF (Waters Corporation). Fourier transform infrared spectroscopy (FT-IR) data were collected on KBr pellet samples in the range of 4000–400 cm^{-1} using an IS-50 FT-IR spectrometer. Thermogravimetric analysis (TGA) was performed at a heating rate of 10 °C·min^{-1} under an Ar flow using a TG/DTA Q600 system.

Magnetic properties measurements. Magnetic susceptibility data were collected using a Quantum Design MPMS XL-5 or PPMS-9T (EC-II) SQUID magnetometer. Measurements for all the samples were performed on microcrystalline powder restrained by a parafilm and loaded in a capsule. The magnetic susceptibility data were corrected for the diamagnetism of the samples using Pascal constants and the sample holder and parafilm by corrected measurement.

X-ray Data Collection and Structure Determinations. Crystals suitable for single crystal X-ray diffraction were covered in a thin layer of hydrocarbon oil, mounted on a glass fiber attached to a copper pin, and placed under an N_2 cold stream. The single-crystal XRD data for two compounds were collected on Bruker D8 Venture CMOS-based diffractometer (Mo-*K*α radiation, λ = 0.71073 Å) using the SMART and SAINT programs. Final unit cell parameters were based on all observed reflections from integration of all frame data. The structures were solved with the ShelXT structure solution program using Intrinsic Phasing and refined with the ShelXL refinement package using Least Squares minimization that implanted in Olex2. For all compounds, all non-hydrogen atoms were refined anisotropically and the hydrogen atoms of organic ligands were located geometrically and fixed isotropic thermal parameters. For detailed information of crystal data, data collection, solution, and refinement, see Table S1.

Powder X-ray diffraction. The crystals of **1** were pulverized in hydrocarbon oil, mounted on glass fibers attached to a copper pin, and powder XRD data were collected on a Bruker D8 Venture CMOS-based diffractometer (Cu-*K*α radiation) using the Phi 360 operation. For three rounds of data, the distance between the instrument and the sample was 240 mm and the acquisition time was 120 s in each round. The 2θ angles used when collecting the three rounds of data were −15°, −30° and −45°, respectively. XRD pattern of **2** was obtained on a D8 ADVANCE X-ray powder diffractometer with Cu *K*α radiation in the angular range 5–50° at room temperature.

SI1.2 Materials

The substrates and reagents, 6,6'-dimethyl-2,2'-bipyridine, chromium(VI) oxide, 2-aminoethan-1-ol, sulfurous dichloride, and sodium hydride, were purchased from Shanghai Aladdin Bio-chem Technology co., ltd. All reagents and solvents were purchased commercially and used as supplied, unless otherwise stated. THF was further dried over sodium benzophenone ketyl, distilled onto $LiAlH_4$ under nitrogen, and distilled under high vacuum just before use. Toluene was dried over anhydrous calcium hydride and distilled before use.

Caution! *Although not encountered in our experiments, perchlorate salts in the presence of organic ligands are potentially explosive. Only a small amount of the materials should be prepared and handled with care.Particularly, reducing the reaction solution of the perchlorate complexes under reduced pressure should be performed very carefully. Phosphorus pentasulfide is toxic. It should be used cautiously.*

SI2 NMR spectra of intermediates and ligand

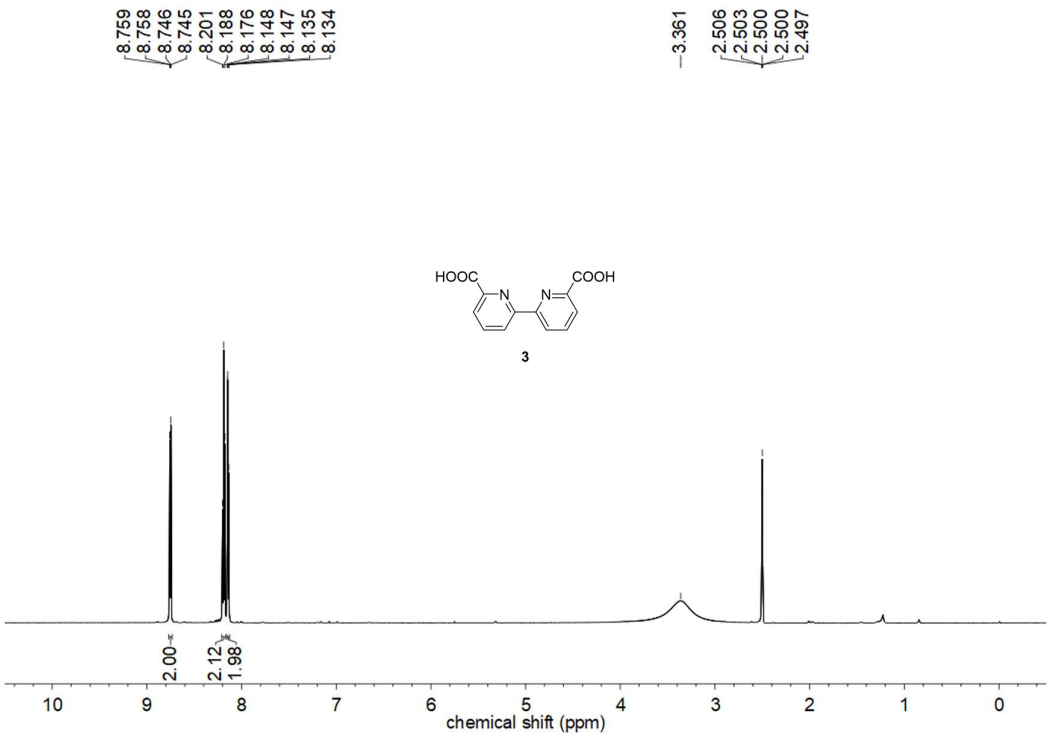

Fig. S1 ^{1}H NMR spectrum of compound **3** (600 MHz) in $CDCl_3$.[1]

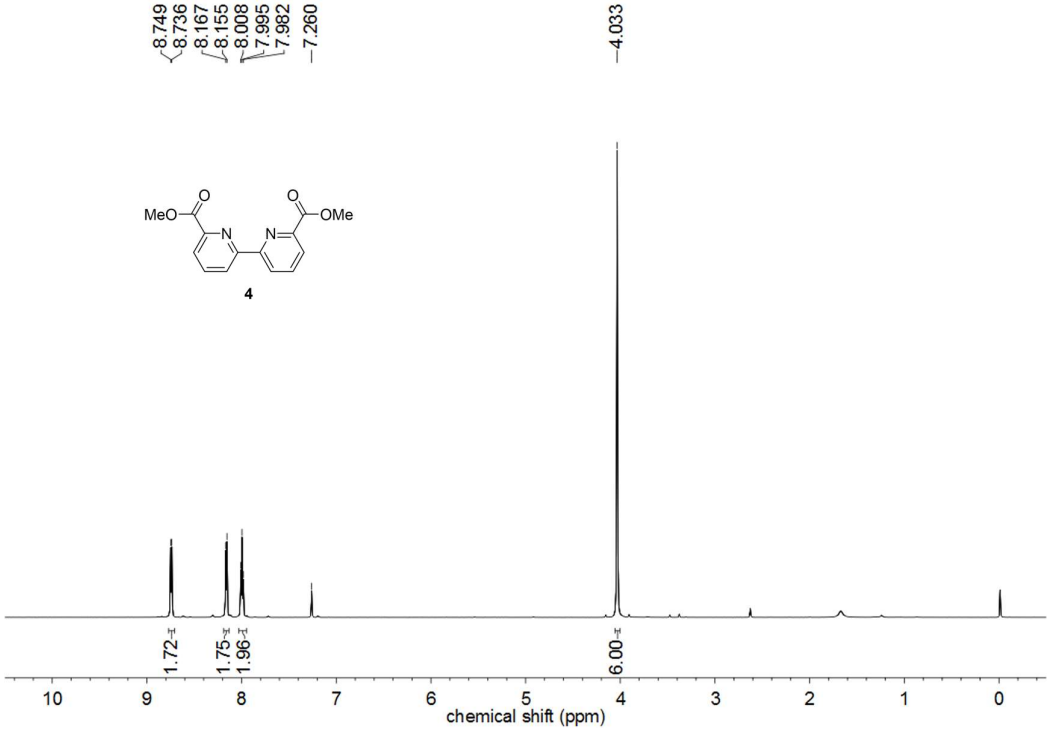

Fig. S2 ^{1}H NMR spectrum of compound **4** (600 MHz) in $CDCl_3$.[2]

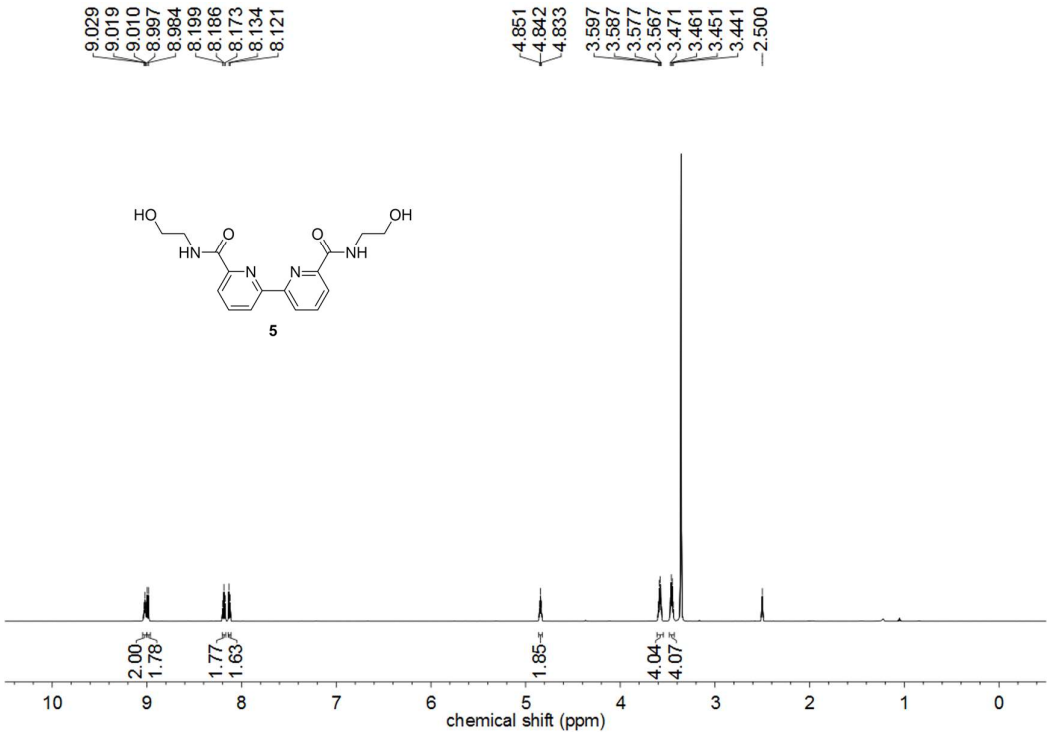

Fig. S3 ^{1}H NMR spectrum of compound **5** (600 MHz) in $CDCl_3$.

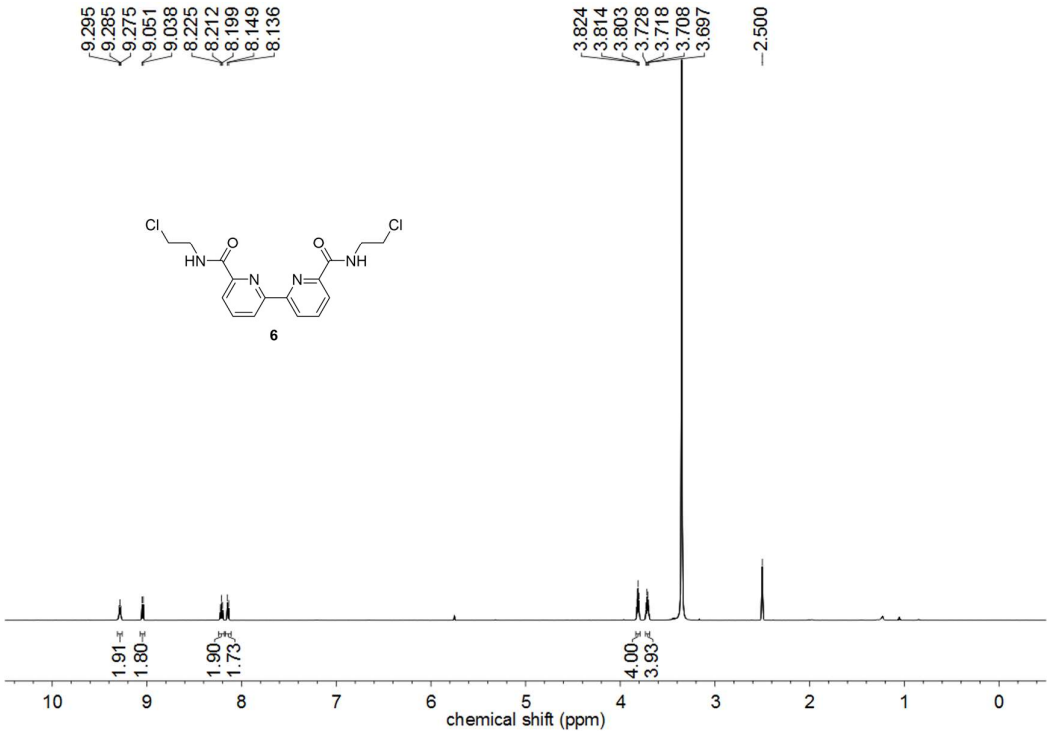

Fig. S4 ^{1}H NMR spectrum of compound **6** (600 MHz) in $CDCl_3$ (10 mM).

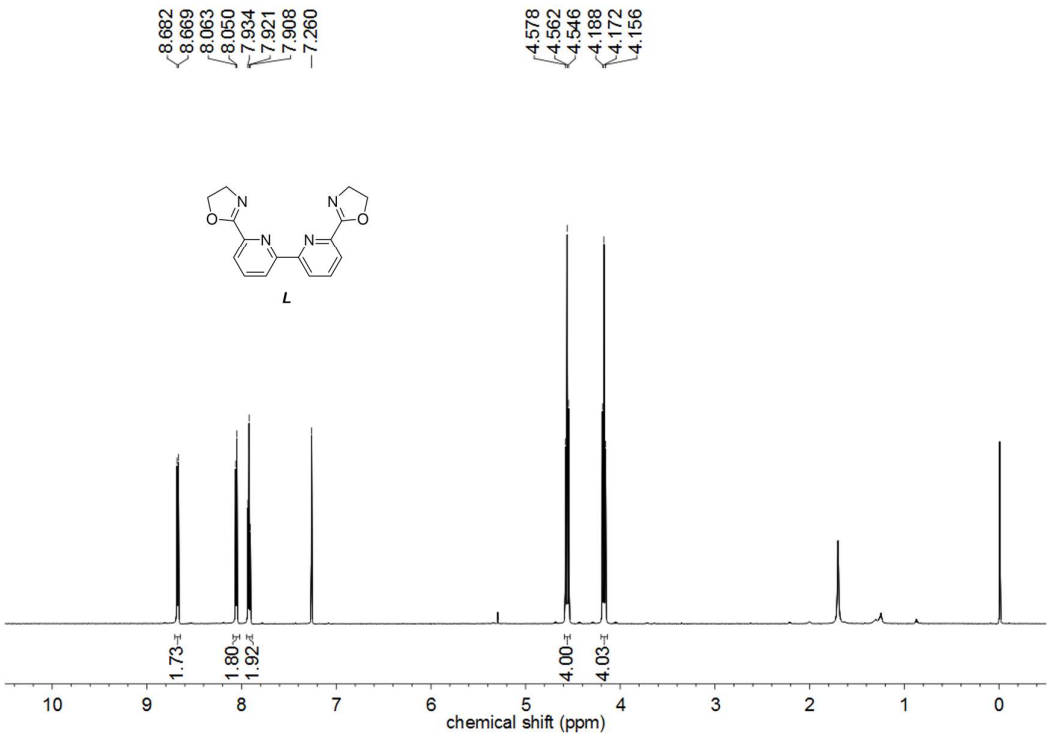

Fig. S5 ^{1}H NMR spectrum of compound ***L*** (600 MHz) in $CDCl_3$.

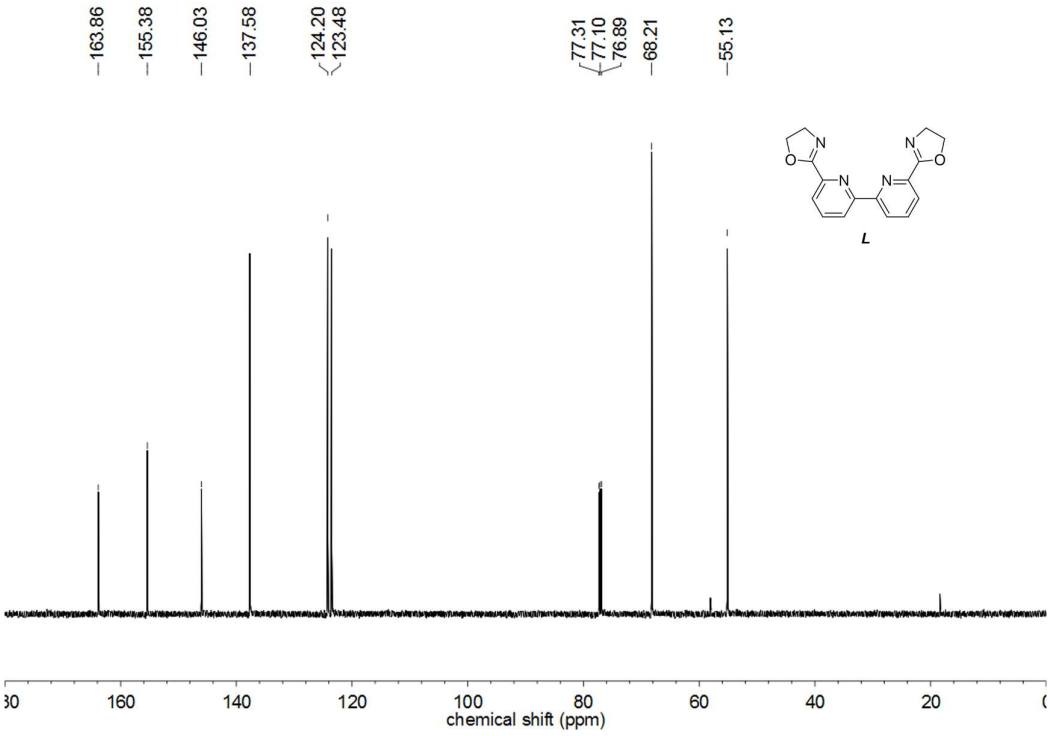

Fig. S6 ^{13}C NMR spectrum of compound ***L*** (125 MHz) in $CDCl_3$.

SI3 Structural details of the complexes

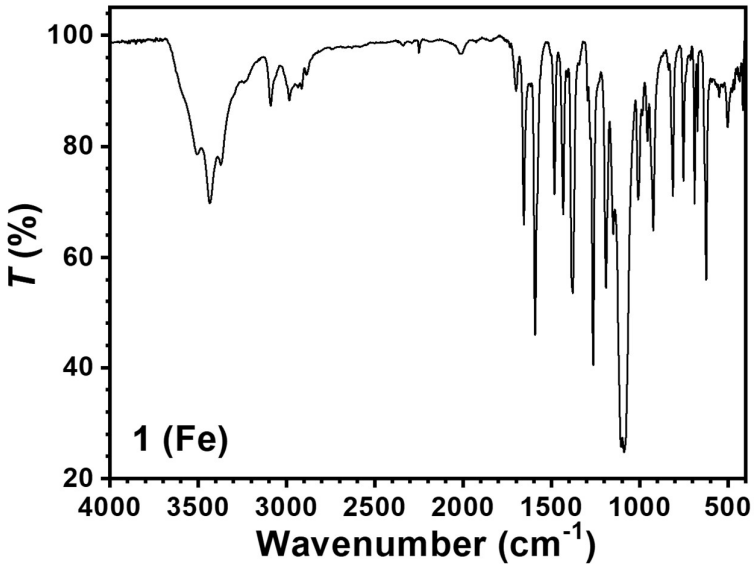

Fig. S7 FT-IR spectrum of complex **1** (KBr pellet).

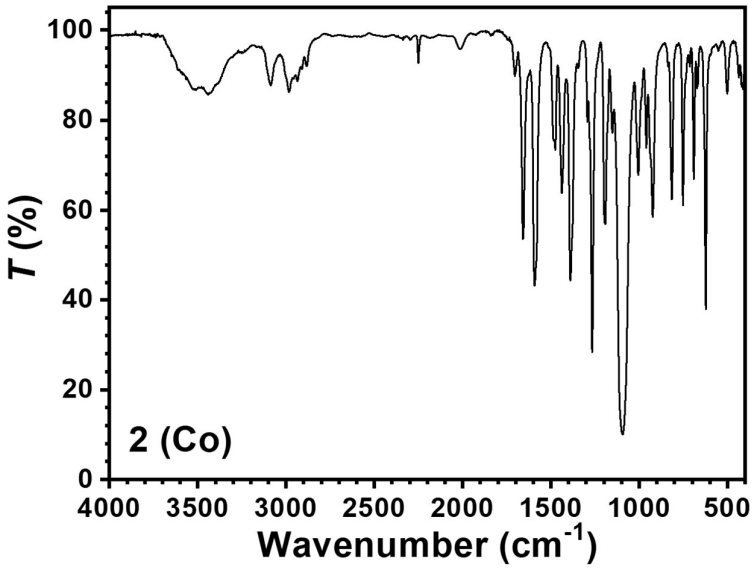

Fig. S8 FT-IR spectrum of complex **2** (KBr pellet).

Table S1. Crystal data, data collection, solution, and refinement information of complexes in this work.

	1	**2**
Formula	$C_{66}H_{59}Cl_4Fe_2N_{17}O_{24}$	$C_{36}H_{34}Cl_2CoN_{10}O_{12}$
Formula weight	1727.80	928.56
Crystal system	Monoclinic	Monoclinic
Space group	$P2_1/n$	$P2_1/c$
a, Å	25.844(3)	15.5153(11)
b, Å	8.7570(11)	14.5762(10)
c, Å	31.467(3)	17.6396(12)
α, deg	90	90
β, deg	101.692(4)	97.136(2)
γ, deg	90	90
V, Å^3	6973.6(14)	3958.4(5)
Z	4	4
T, K	120.0	120.0
F(000)	3544.0	1908.0
D_C, g cm^{-3}	1.646	1.558
μ, mm^{-1}	0.665	0.645
λ, Å	0.71073	0.71073
crystal size, mm^3	0.20 × 0.04 × 0.02	0.10 × 0.10 × 0.08
T_{min} and T_{max}	0.878, 0.987	0.938, 0.950
θ_{min}, θ_{max}, deg	2.286, 27.507	2.646, 27.517
no. total reflns.	90316	39618
no. uniq. reflns, R_{int}	16122, 0.0765	9046, 0.0363
no. obs. [$I \geq 2\sigma(I)$]	11308	7084
no. params	1019	552
$R1$ [$I \geq 2\sigma(I)$]	0.0440	0.0403
$wR2$ (all data)	0.1066	0.1118
S	1.019	1.033
$\Delta\rho$,[a] e/Å^3	0.748, –0.599	0.640, –0.765
max. and mean Δ/σ[b]	0.001, 0.000	0.001, 0.000
CCDC	2154726	2154727

[a] Max and min residual density. [b] Max and mean shift/σ.

Table S2. Selected bond angles (°) for **1** and **2**.

1		**1**		**2**	
No	angles (°)	No	angles (°)	No	angles (°)
N1–Fe1–N2	70.13(8)	N9–Fe2–N10	69.22(7)	N1–Co1–N2	71.84(6)
N1–Fe1–N3	135.77(8)	N9–Fe2–N11	134.66(7)	N1–Co1–N3	139.77(6)
N1–Fe1–N5	90.93(8)	N9–Fe2–N12	155.69(7)	N1–Co1–N5	90.03(6)
N1–Fe1–N6	77.89(8)	N9–Fe2–N13	90.03(8)	N1–Co1–N6	75.46(6)
N1–Fe1–N7	80.18(8)	N9–Fe2–N14	78.24(7)	N1–Co1–N7	75.38(6)
N1–Fe1–N8	96.07(8)	N9–Fe2–N15	81.18(7)	N1–Co1–N8	92.54(6)
N2–Fe1–N3	65.92(8)	N9–Fe2–N16	96.99 (8)	N2–Co1–N3	67.94(6)
N2–Fe1–N6	136.33(7)	N10–Fe2–N11	65.62(8)	N2–Co1–N6	137.32(6)
N2–Fe1–N7	133.17(8)	N12–Fe2–N10	135.00(8)	N2–Co1–N7	135.33(6)
N3–Fe1–N6	134.08(8)	N12–Fe2–N11	69.40(8)	N3–Co1–N6	137.60(6)
N3–Fe1–N7	135.79(7)	N12–Fe2–N14	79.82(7)	N3–Co1–N7	137.41(6)
N4–Fe1–N1	154.34(8)	N12–Fe2–N15	80.45(8)	N4–Co1–N1	148.36(6)
N4–Fe1–N2	135.53(8)	N12–Fe2–N16	91.31(8)	N4–Co1–N2	139.80(6)
N4–Fe1–N3	69.76(8)	N13–Fe2–N10	81.13(7)	N4–Co1–N3	71.86(6)
N4–Fe1–N5	93.21(8)	N13–Fe2–N11	79.46(7)	N4–Co1–N5	91.35(6)
N4–Fe1–N6	79.83(7)	N13–Fe2–N12	92.15(8)	N4–Co1–N6	76.24(6)
N4–Fe1–N7	79.16(8)	N13–Fe2–N14	69.83(7)	N4–Co1–N7	77.40(6)
N4–Fe1–N8	90.76(8)	N13–Fe2–N15	135.90(7)	N4–Co1–N8	90.76(7)
N5–Fe1–N2	81.51(8)	N13–Fe2–N16	154.63(7)	N5–Co1–N2	86.93(6)
N5–Fe1–N3	78.18(7)	N14–Fe2–N10	136.00(7)	N5–Co1–N3	87.11(6)
N5–Fe1–N6	69.86(8)	N14–Fe2–N11	135.26(8)	N5–Co1–N6	66.27(6)
N5–Fe1–N7	135.53(7)	N14–Fe2–N15	66.07(7)	N5–Co1–N7	122.79(6)
N5–Fe1–N8	155.02(8)	N15–Fe2–N10	133.04(8)	N5–Co1–N8	171.42(6)
N7–Fe1–N6	65.67(7)	N15–Fe2–N11	134.88(7)	N7–Co1–N6	56.54(6)
N8–Fe1–N2	78.44(7)	N16–Fe2–N10	78.70(7)	N8–Co1–N2	86.10(6)
N8–Fe1–N3	80.12(8)	N16–Fe2–N11	78.29(8)	N8–Co1–N3	85.64(6)
N8–Fe1–N6	135.06(8)	N16–Fe2–N14	135.46(7)	N8–Co1–N6	122.31(6)
N8–Fe1–N7	69.42(7)	N16–Fe2–N15	69.43(7)	N8–Co1–N7	65.79(6)

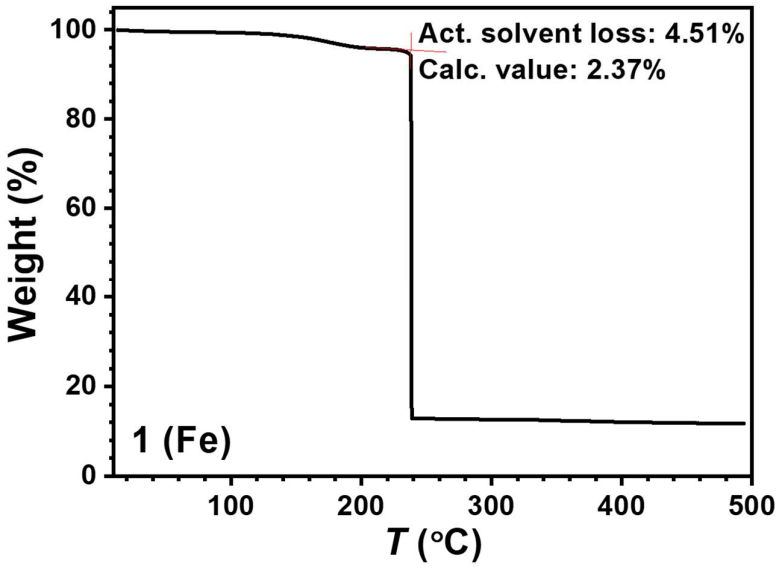

Fig. S9 TGA trace of **1** from ambient temperature to 500 °C.

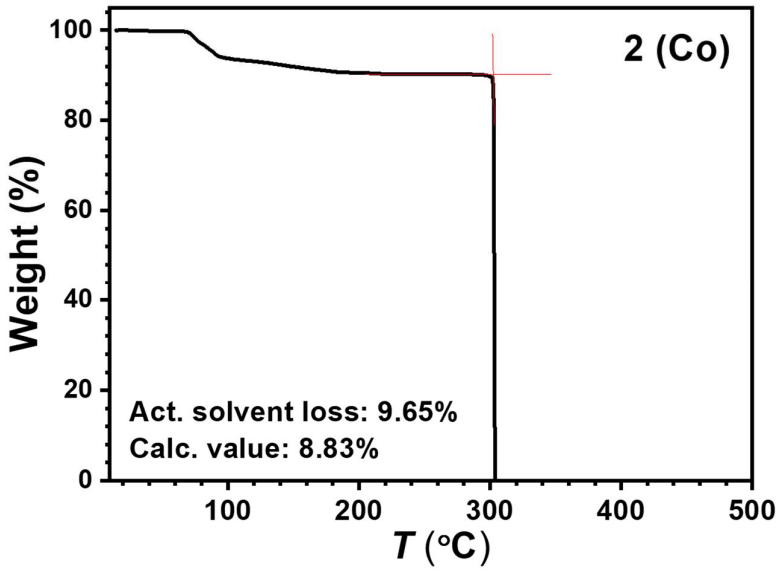

Fig. S10 TGA trace of **2** from ambient temperature to 500 °C.

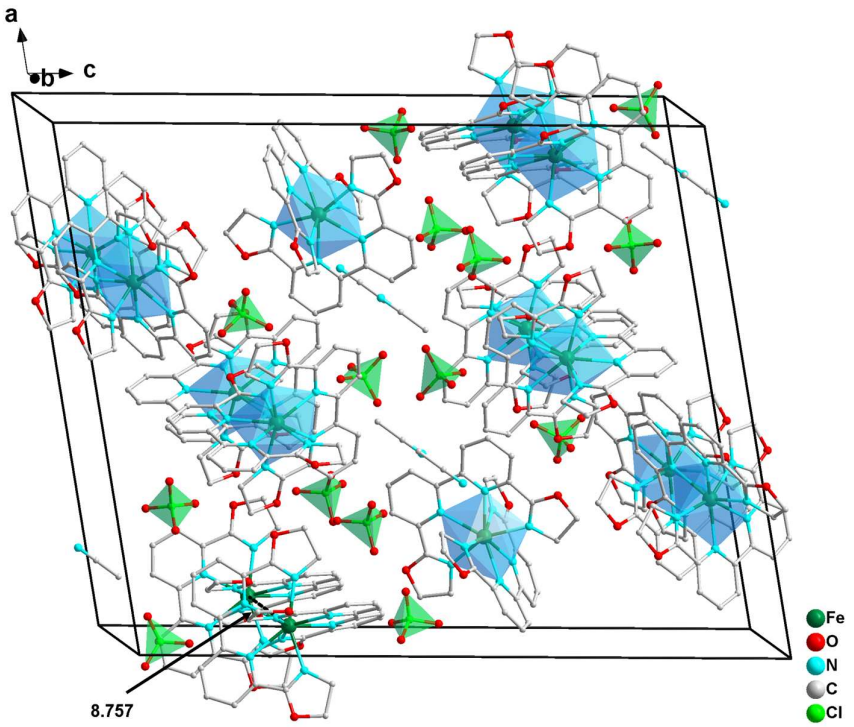

Fig. S11 Projection of the unit-cell of **1** along *b* axis at 120 K.

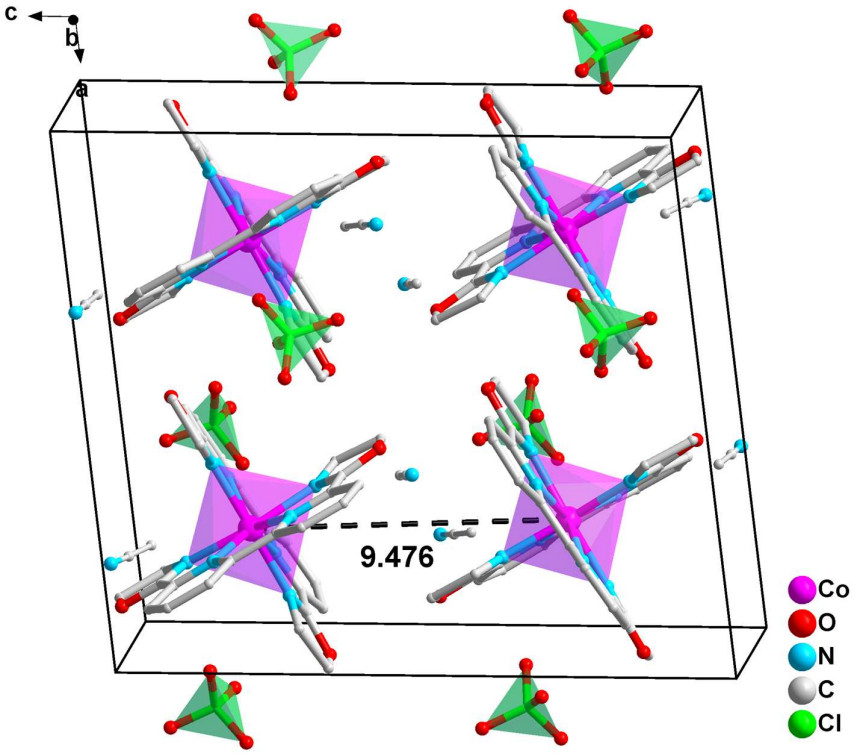

Fig. S12 Projection of the unit-cell of **2** along *b* axis at 120 K.

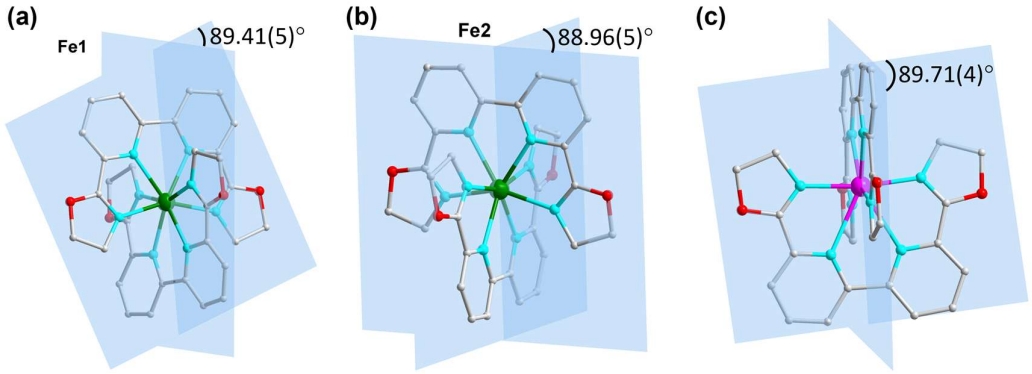

Fig. S13 The calculated included angles between two ligand planes of (a) Fe1 in **1**, (b) Fe2 in **1**, and (c) Co in **2**, respectively.

Table S3. Selected geometrical parameters for **1** and **2**.[3]

Shape	Symmetry	Fe1	Fe2	Co1
OP-8	D_{8h}	31.568	31.611	31.598
HPY-8	C_{7v}	25.972	25.838	26.788
HBPY-8	D_{6h}	14.474	14.177	13.894
CU-8	O_h	12.169	12.023	12.038
SAPR-8	D_{4d}	3.445	3.319	4.837
TDD-8	D_{2d}	1.312	1.253	2.608
JGBF-8	D_{2d}	10.720	10.469	8.871
JETBPY-8	D_{3h}	27.287	27.792	25.069
JBTPR-8	C_{2v}	2.910	2.906	3.426
BTPR-8	C_{2v}	2.433	2.495	3.580
JSD-8	D_{2d}	2.346	2.277	1.778
TT-8	T_d	12.968	12.793	12.855
ETBPY-8	D_{3h}	23.632	24.195	22.234

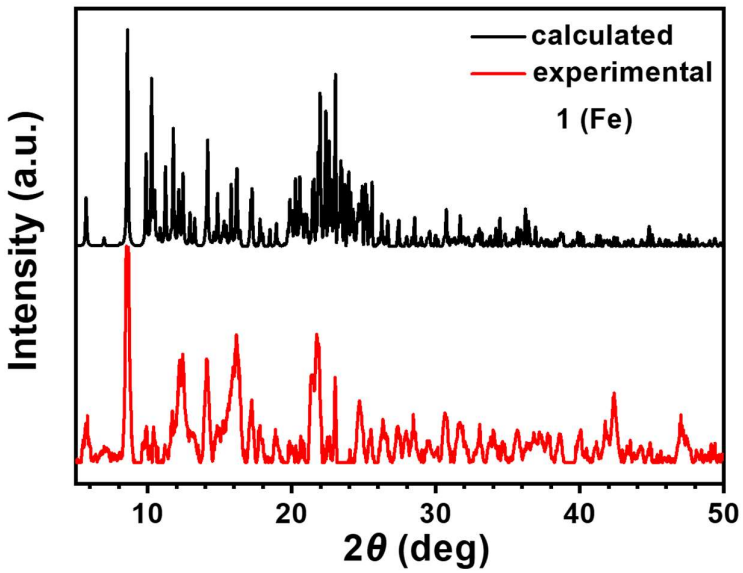

Fig. S14 The powder XRD pattern of compound **1** and the simulated one based on the single-crystal structure.

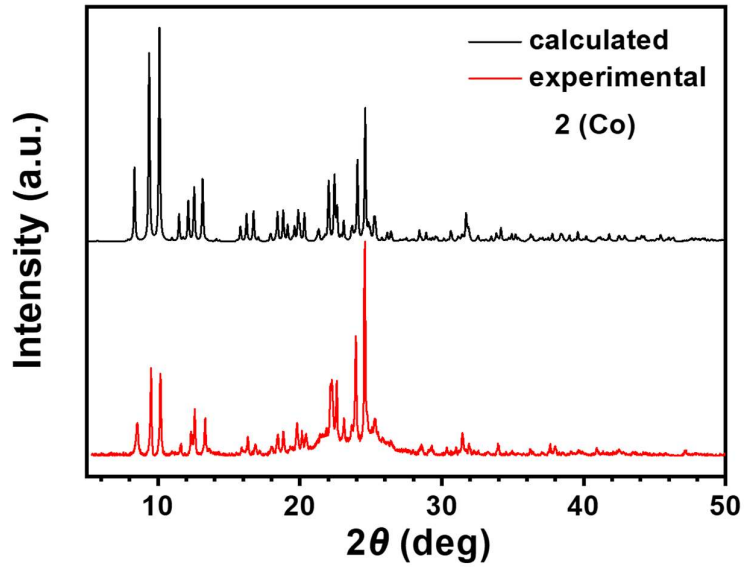

Fig. S15 The powder XRD pattern of compound **2** and the simulated one based on the single-crystal structure.

SI4 Supplementary magnetic characterization

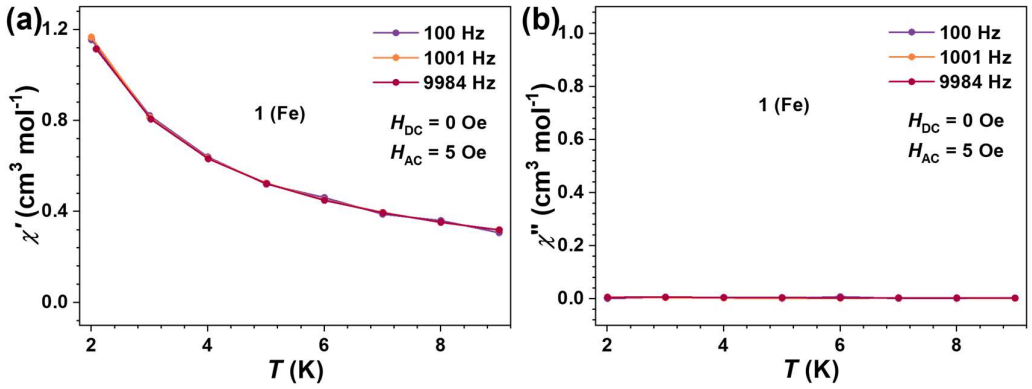

Fig. S16 Temperature dependence of in-phase (χ') and out-of-phase (χ'') of **1** at different frequencies in the absence of dc field, no obvious frequency dependence can be observed.

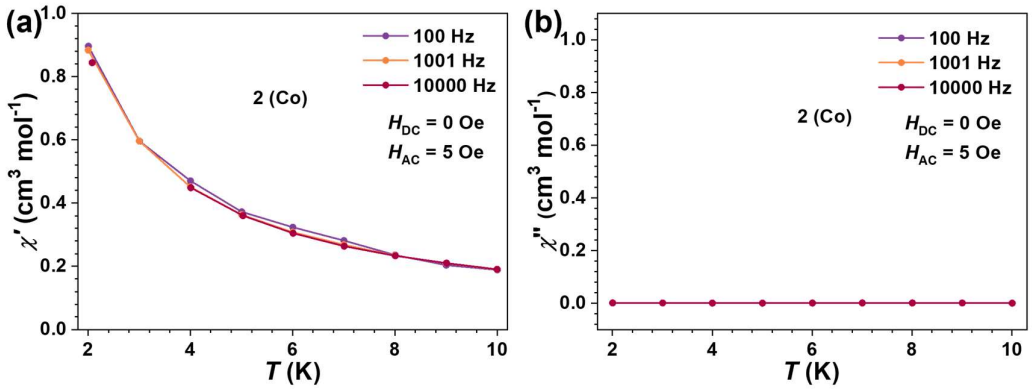

Fig. S17 Temperature dependence of in-phase (χ') and out-of-phase (χ'') of **2** at different frequencies in the absence of dc field, no obvious frequency dependence can be observed.

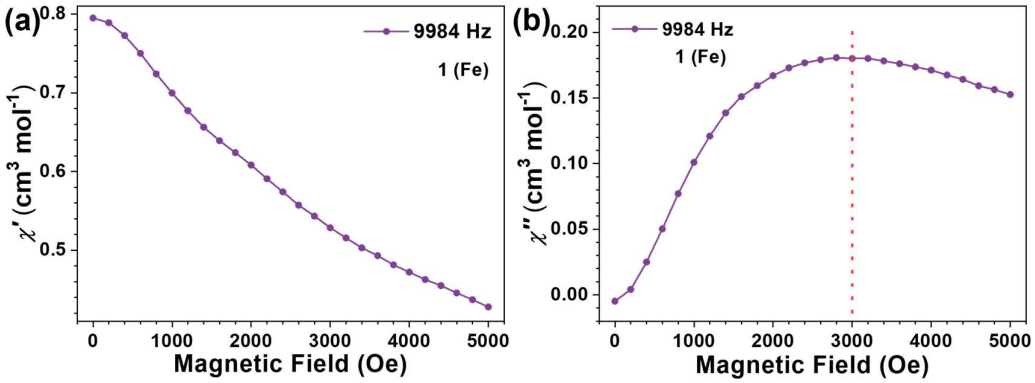

Fig. S18 Field dependence of (a) in-phase (χ') signal and (b) out-of-phase (χ'') signal of the ac magnetic susceptibility for **1** (H_{AC} = 5 Oe).

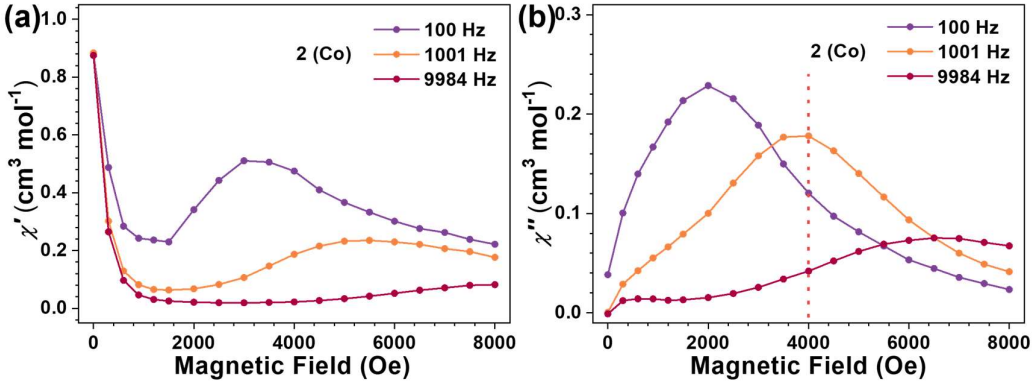

Fig. S19 Field dependence of (a) in-phase (χ') signal and (b) out-of-phase (χ'') signal of the ac magnetic susceptibility for **2** (H_{AC} = 5 Oe).

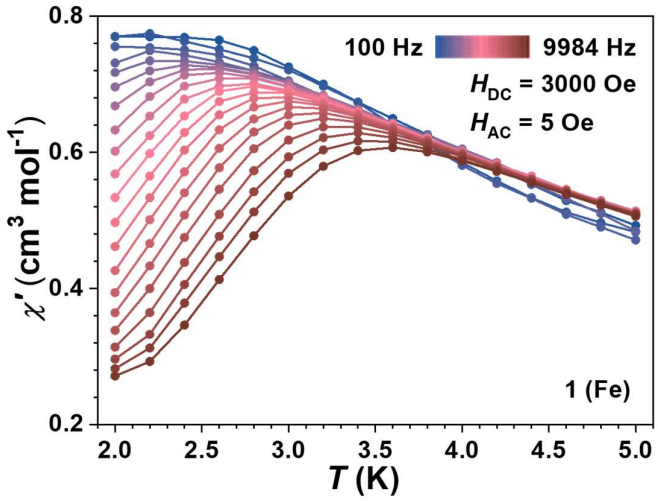

Fig. S20 Temperature dependences of the in-phase (χ') ac susceptibilities for **1** under 3000 Oe dc field (H_{AC} = 5 Oe).

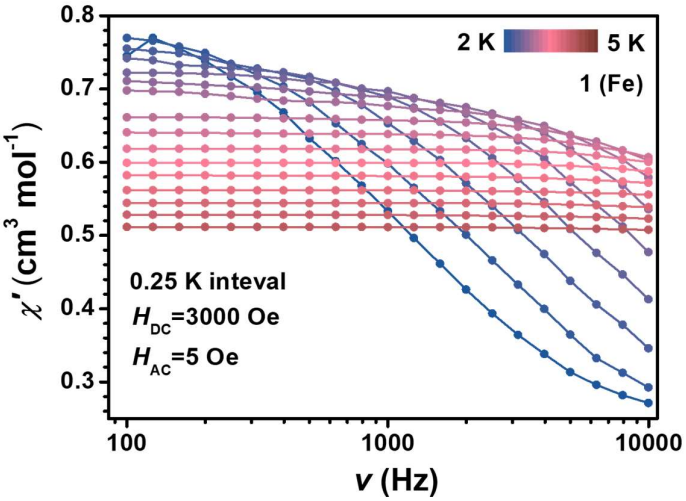

Fig. S21 Frequency dependences of the in-phase (χ') ac susceptibilities for **1** under 3000 Oe dc field (H_{AC} = 5 Oe).

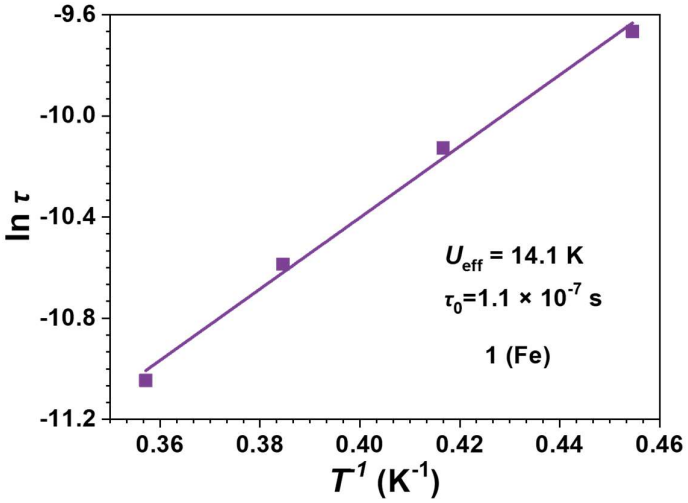

Fig. S22 Arrhenius plots of relaxation times of **1** under a dc field of 3000 Oe. The data was collected from the peaks of χ'' (out-of-phase) against temperature at different frequencies.

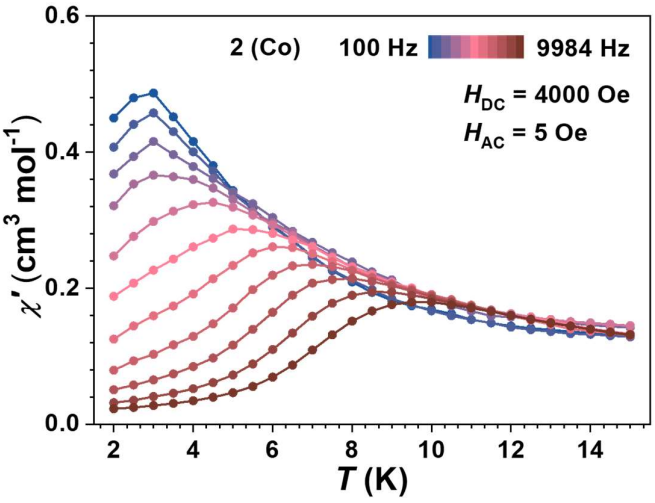

Fig. S23 Temperature dependences of the in-phase (χ') ac susceptibilities for **2** under 4000 Oe dc field (H_{AC} = 5 Oe).

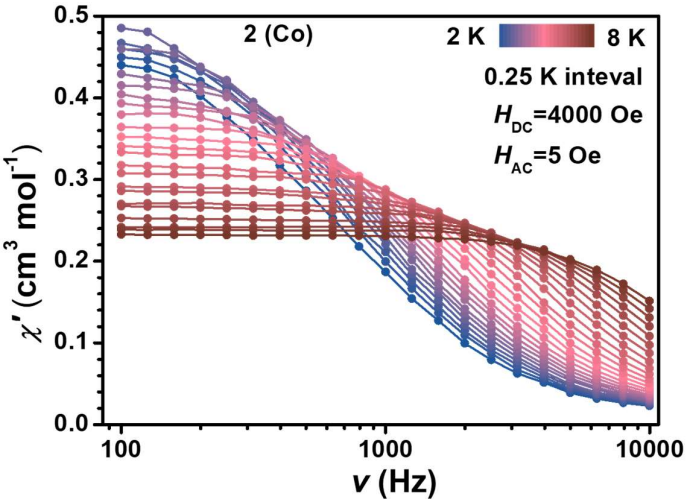

Fig. S24 Frequency dependences of the in-phase (χ') ac susceptibilities for **2** under 4000 Oe dc field (H_{AC} = 5 Oe).

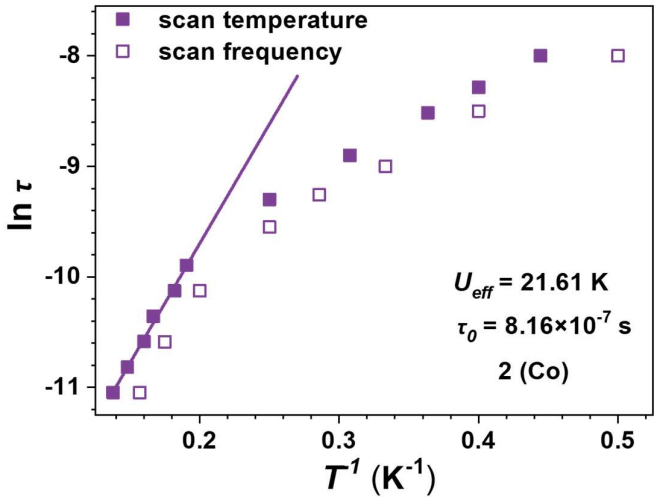

Fig. S25 Arrhenius plots of relaxation times of **2** under a dc field of 4000 Oe. The data was collected from the peaks of χ'' (out-of-phase) against temperature and the peaks of χ'' (out-of-phase) against frequency at different temperatures.

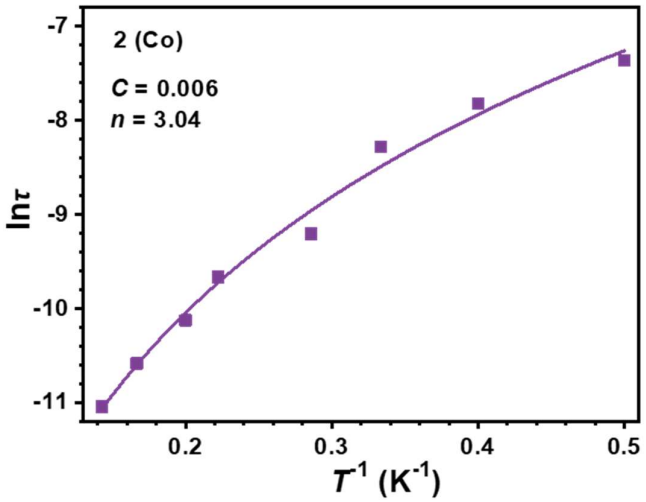

Fig. S26 The fitting of ln τ *vs*. T^{-1} plots by applying the Raman process, which gives $C = 0.006$ and $n = 3.04$ with $R^2 = 0.987$.

Table S4. The parameters of Cole-Cole fitting of **1** under 3000 Oe applied dc field.

T (K)	X_s (cm^3 mol^{-1})	X_t (cm^3 mol^{-1})	(s)	α	R
2.00	0.21245	0.83383	0.00001	0.30245	5.79×10^{-4}
2.20	0.18437	0.80256	0.00001	0.32792	3.73×10^{-4}
2.40	0.18832	0.77193	0.00001	0.27993	4.01×10^{-4}
2.60	0.12520	0.76394	0.00001	0.36651	6.93×10^{-4}
2.80	0.17156	0.73204	0.00001	0.25034	2.37×10^{-4}
3.00	0.01494	0.71559	0.00001	0.32378	6.23×10^{-4}

Table S5. The parameters of Cole-Cole fitting of **2** under 4000 Oe applied dc field.

T (K)	X_s (cm^3 mol^{-1})	X_t (cm^3 mol^{-1})	(s)	α	R
2.00	0.00396	0.50351	0.00001	0.19704	8.77×10^{-5}
2.25	0.00298	0.52538	0.00001	0.23269	1.37×10^{-4}
2.50	0.00162	0.53235	0.00001	0.20973	1.96×10^{-4}
2.75	0.00211	0.51640	0.00001	0.19677	2.44×10^{-4}
3.00	0.00109	0.52128	0.00001	0.20823	1.15×10^{-4}
3.25	0.00840	0.47561	0.00001	0.14945	3.31×10^{-5}
3.50	0.01188	0.45121	0.00001	0.12194	3.22×10^{-4}
3.75	0.01264	0.43765	0.00001	0.12165	7.03×10^{-4}
4.00	0.01354	0.41470	0.00001	0.11020	3.01×10^{-4}
4.25	0.01772	0.40221	0.00001	0.08505	6.32×10^{-4}
4.50	0.01744	0.38744	0.00001	0.08670	4.02×10^{-4}
4.75	0.01933	0.37361	0.00170	0.07564	1.16×10^{-3}
5.00	0.01959	0.35903	0.00001	0.07357	6.46×10^{-4}
5.25	0.01841	0.34497	0.00001	0.07304	2.08×10^{-4}
5.50	0.01035	0.33708	0.00001	0.11026	8.66×10^{-5}
5.75	0.01173	0.31999	0.00001	0.08841	2.33×10^{-4}
6.00	0.00942	0.31032	0.00001	0.09383	5.16×10^{-5}
6.25	0.03902	0.28915	0.07541	-0.02716	1.14×10^{-3}
6.50	-0.00155	0.28775	0.00001	0.10557	1.86×10^{-4}
6.75	0.03245	0.27017	0.61191	-0.00493	4.64×10^{-4}
7.00	0.04241	0.26220	0.00269	-0.03093	3.83×10^{-4}
7.25	0.03383	0.25019	0.00001	-0.02910	8.08×10^{-5}
7.50	0.04613	0.24100	0.00001	-0.06648	1.46×10^{-3}
7.75	0.04718	0.23608	0.00203	-0.06140	1.12×10^{-3}
8.00	0.03974	0.23036	0.00012	-0.03426	1.91×10^{-4}

SI5 Supplementary theoretical calculation details

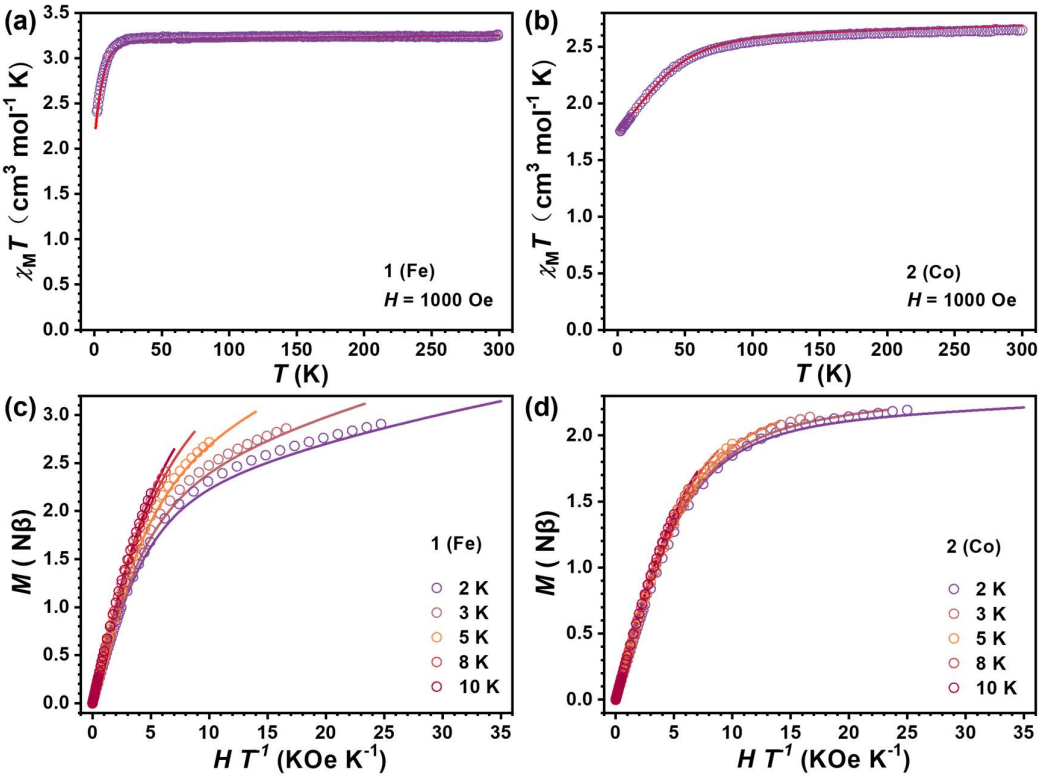

Fig. S27 Experimental and theoretical $\chi_M T$ *vs*. *T* plots under 1000 Oe applied dc field at 2–300 K for **1** (a) and **2** (b). Experimental and theoretical *M vs*. *H/T* plots at different temperatures (2, 3, 5, 8 and 10 K) for **1** (c) and **2** (d). The solid line represents the calculated magnetic susceptibilities by the CASSCF/NEVPT2/QDPT methods using the ORCA-5.0.2 package.

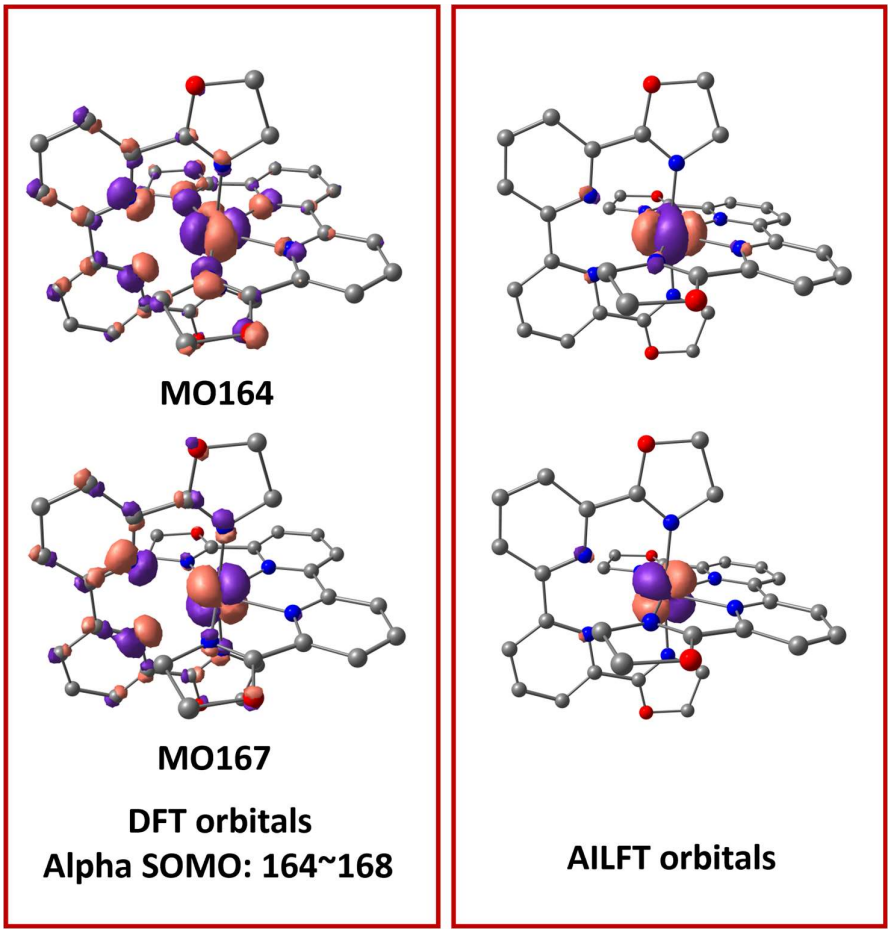

Fig. S28 DFT molecular orbitals and AILFT orbitals showing orbital interaction between the long-distance Co-N(py) atom pairs. Contour value is set to 0.1. (Left) alpha spin orbitals from DFT calculations (BP86/def2-TZVP/D3BJ). Decomposition with Mulliken partition method yields ~36% from Co and ~10% from each of the two N atoms. (Right) AILFT orbitals based on CASSCF/NEVPT2 calculations.

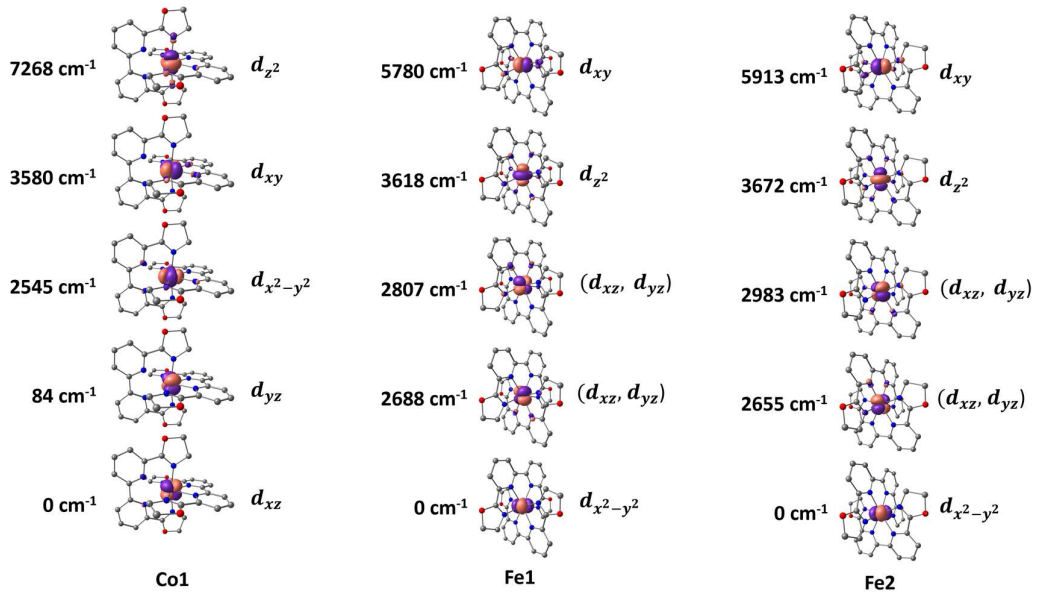

Fig. S29 AILFT 3d orbitals and corresponding energy of Co1(left), Fe1(middle), Fe2(right) fragments. The *d*-orbital assignment is in the zero-field splitting tensor (***D*** tensor) frame.

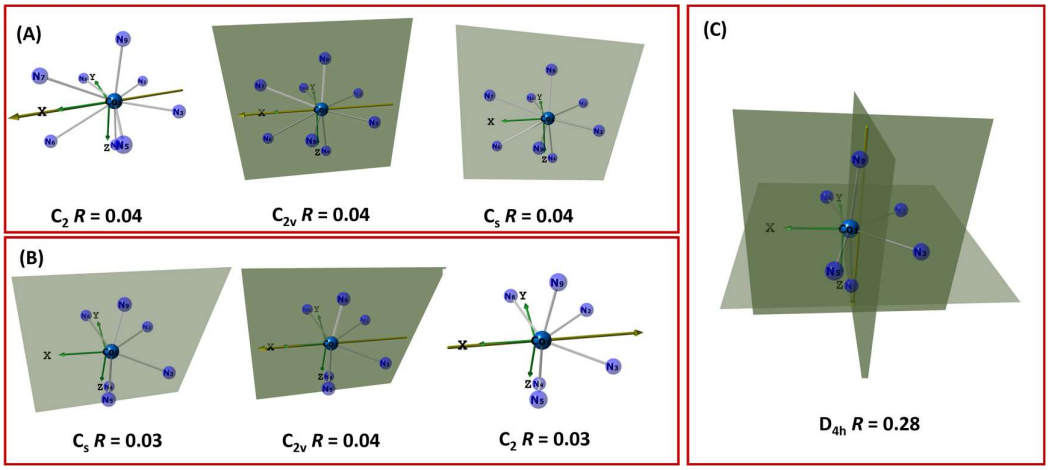

Fig. S30 Point group analysis on CoN_8 or CoN_6 moiety. (A) three point groups with smallest R values for CoN_8; (B) three point groups with smallest *R* values for CoN_6; (C) the closest point group (smallest *R*) consistent with the zero-field splitting ***D*** tensor frame.

SI6 References

1. G. Bozoklu, C. Marchal, C. Gateau, J. Pécaut, D. Imbert and M. Mazzanti, *Chem. Eur. J.*, 2010, **16**, 6159-6163.
2. F. Forato, A. Belhboub, J. Monot, M. Petit, R. Benoit, V. Sarou-Kanian, F. Fayon, D. Jacquemin,

C. Queffelec and B. Bujoli, *Chem. Eur. J.*, 2018, **24**, 2457-2465.

3. M. Llunell, D. Casanova, J. Cirera, P. Alemany and S. Alvarez, *SHAPE, version 2.0,* , 2010, Universitat de Barcelona, Barcelona, Spain.